

Densitometry test of bone tissue: Validation of computer simulation studies

M. Binkowski^{a,*}, E. Tanck^b, M. Barink^b, W.J. Oyen^c, Z. Wrobel^a, N. Verdonschot^{b,d}

^aDepartment of Biomedical Computer Systems, Institute of Computer Science, Faculty of Computer and Material Science, University of Silesia, ul. Będzińska 39, Sosnowiec, Poland

^bOrthopaedic Research Laboratory, Radboud University Nijmegen Medical Centre, Nijmegen, The Netherlands

^cDepartment of Nuclear Medicine, Radboud University Nijmegen Medical Centre, Nijmegen, The Netherlands

^dDepartment of Bioengineering, University of Twente, The Netherlands

Received 26 April 2007; accepted 2 April 2008

Abstract

Bone densitometry measurements are performed to predict the fracture risk in bones. However, the sensitivity of these predictions are not satisfactory. One of the explanations is that densitometry ignores the (architectural) structural aspects of the bone. The effects of varying architectural parameters on the densitometry parameters can be effectively assessed by considering a 3-D image of a bone and vary the bone structure parameters in a controlled manner and determine the consequence of these changes on a simulated (virtual) densitometry analysis.

In this paper we present such a computer simulation of densitometry analysis of bone. The simulation allows quantification of densitometry parameters, such as BMD and BMC, on the basis of computed tomography bone scans. The aim of the presented study is the evaluation of our method by comparing its results to the results from real densitometry (DEXA) tests.

For the evaluation we selected three femoral bones. These items were CT scanned and individual computer models were created. In addition, the densitometry parameters of these items were assessed by a clinical DEXA scanner.

The densitometry parameters obtained from the simulations were very close to the results from the DEXA densitometry measurements. We therefore conclude that our method can be employed in the research on the influence of changes in bone structure on densitometry test results. Crown Copyright © 2008 Published by Elsevier Ltd. All rights reserved.

Keywords: X rays; Computer simulation; Attenuation coefficient; Bone model; Bone mineral density; Bone mineral content

1. Introduction

A densitometry test forms the basis for the diagnosis of bone susceptibility to fractures. Such a test can be performed using a number of techniques. The World Health Organisation [1] and International Osteoporosis Foundation guidelines currently recommend dual energy X-ray absorptiometry (DEXA) as a convenient and reliable manner to conduct a densitometry test of the proximal femur [2–6].

An alternative method of diagnosing osteoporosis is quantitative computed tomography (QCT) [7]. This method delivers information about physical bone density per unit of volume. Furthermore, QCT allows separate measurements of cortical

and trabecular bone densities. Although QCT is the most precise method for measuring bone density, it is less economical due to higher hardware and running costs (in comparison to DEXA equipment) and therefore not practical in screening tests [8].

Some studies suggest that there is a close correlation between the bone mineral density (BMD) and the risk of a fracture [7,9]. However, other studies suggest that the absolute number of fractures does not solely depend on BMD. In a study reported by Burger et al. 63% of the fractured cases had an average or slightly osteopenic BMD [10]. Similar results were reported by Nowak and Badurski [34].

When using the DEXA method, the characteristic unit is the BMD measured as g/cm^2 [7,12–15]. Due to the two-dimensional character of the data medium—a bone image—measuring mass quantity per volume unit is impossible. Moreover, only the sum of projected (cortical and trabecular) bone is presented and the resolution of the method does not allow taking into consideration the structure of the bone.

* Corresponding author. ul. Biniszkievicza 37 40-300 Katowice, Poland. Tel.: +48 501296516.

E-mail addresses: marcin.binkowski@us.edu.pl, binkowsk@wp.pl (M. Binkowski).

Consequently, all the information about bone structure remains unattainable. As a result of this, DEXA could produce similar densitometry values for bones with similar density distributions but with very different structures. The internal structure of (trabecular) bone is essential for load transfer which explains that DEXA measurements cannot be fully predictive of bone failure.

In order to explain the mechanism of discrepancies between densitometry test results and real bone strength, it should be quantitatively demonstrated which changes in bone tissue microstructure can lead to misleading densitometry test results. This can be most efficiently done using computer simulations of X-ray propagation of virtual bone samples. The structure of the samples can be varied much easier than real test samples and it can be assessed whether there is any effect of the changed structure on the densitometry parameters. Before these analyses can be done, it is essential to validate the X-ray propagation simulation method against real DEXA measurements. X-ray propagation studies are conducted by various research groups around the world. However, to the best of our knowledge, there are no publications comparing densitometry parameters on the basis of the simulation of X-ray propagation through a bone model created using data from QCT with real DEXA values. The purpose of this paper is to present the X-ray propagation simulation and to validate the outcome parameters with results obtained from real densitometry (DEXA) measurements.

2. Materials and methods

The methods of computer simulation of X-ray radiation propagation are usually considered during studies of medical imaging methods, e.g.: computed tomography, radiography [16–18], mammography [19], dual energy mammography [20]. Moreover, computer simulation was also employed for research on bone tissue densitometry, but only applied to phantoms and not real bone [21,22].

The method that we propose to assess the changes in bone structure and their influence on densitometry test results has previously been described when it was applied to a plate model [23]. In this study the simulation was expanded to simulate X-ray propagation and model the spatial distribution of bone density (which will be abbreviated as the SDBD model).

Previously, some studies on the simulation of X-rays have been conducted employing stochastic models [16,17,19,20,24,25]. We based, however, our approach on deterministic calculations upon the assumption that even without stochastic components the obtained results will be precise enough. We envisage that such a method can be an acceptable simplification of X-ray physics in the case of the research on the densitometry technique.

The implemented SDBD model permitted to define virtual bone tissue and compute the attenuation of X-rays propagated through the virtual bone and recorded in the detector. Based on the distribution of X-ray intensity in the detector the software enabled calculating densitometry parameters in a selected region of interest.

Femoral bone specimens were scanned using quantitative computed tomography. The obtained data was the basis for

defining the SDBD model used in the X-ray propagation computer simulations. In this way we obtained the virtual samples, for which the densitometry parameters were calculated. Then, the real specimens used to define the virtual samples were examined using standard densitometry equipment, which provided us with a reference values for the validation of the X-ray propagation model.

2.1. Specimen selection and preparation

All the tests and procedures with freshly frozen human bones were performed at the Orthopaedic Research Laboratory of the Radboud University Nijmegen Medical Centre (The Netherlands), which has the required permissions to carry out studies with human bodies. The femurs used in the research were taken from cadaver bodies. We selected bones that represented realistic densities as are present in the population; they were selected based on DXA-values. Consequently, we chose a bone with an ‘average’ density (bone no. 1), a mildly osteoporotic one (bone no. 2) and a highly osteoporotic one (i.e. a bone with a very low density) (bone no. 3).

All bones were prepared with the same laboratory process, which included removing all soft tissue. The proximal femur was potted in at the distal side so that it could be oriented such that it was scanned in anterior-posterior direction. The same fixation system ensured that the bone was oriented identical in the CT scanner. The specimens were scanned in a water bath (Fig. 2a), which, according to several studies [26–32], is considered a suitable phantom of soft tissue. The same level of water was maintained during all the scans.

2.2. DEXA scanning

The bones were scanned with a fan beam DEXA machine (QDR4500 Hologic Inc., USA), the results of which were used as the reference values for the comparison with the results from X-ray simulations. For all the tests standard scanner settings were used and densitometry parameters were calculated by the DEXA equipment software. The parameters included the ones that are commonly used in densitometry examinations of patients, namely the BMD (g/cm^2), the bone mineral content (BMC [g]) and the area (Area [cm^2]). The settings used during the DEXA tests are listed in Table 1.

Three femoral bones were scanned with DEXA and the results were obtained from the evaluation of the densitometry

Table 1
The list of the DEXA settings used during scanning

Setting name and unit	Value
Voltage (kVp)	140/100
Current (mA) (avg)	2.5
Scan time (s)	74
Scan length (cm)	15.3
Scan width (cm)	11.4
Line spacing (cm)	0.1008
Point resolution (cm)	0.0901

Table 2
The information about the regions of interest which were set during the tests of the bones*

Name	Size	Description of region
R1 head	Rectangular	From top of head to bottom of head
R2 neck	Rectangular	From top of neck to bottom of head
R3 trochanter	Rectangular	From bottom head to bottom of small trochanter
R4 all	Rectangular	From top of head to bottom of small trochanter

*Right hip for none no. 1 and 3, left hip for bone no. 2.

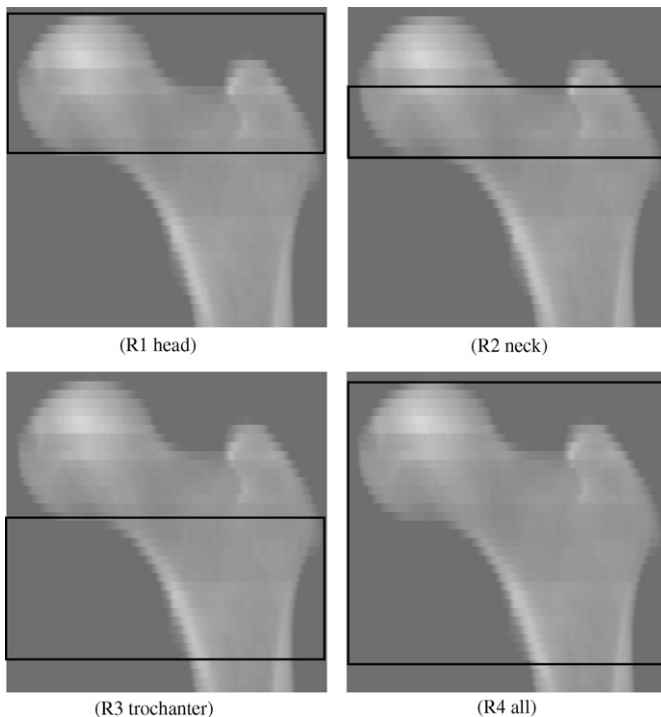


Fig. 1. Diagrams of the DEXA regions (see Table 2) used in the DEXA tests of the bones.

parameters for four different ROIs that were set on the equipment using a free box densitometry module. The ROI called “R1 head” included the whole femoral head from the top of the head to the bottom of the head. The ROI called “R2 neck” included the region from the top of the neck to the bottom of the head. The ROI called “R3 trochanter” covered the region from the bottom of the head to the bottom of the small trochanter. The ROI called “R4 all” included the region from the top of the head to the bottom of the minor trochanter (hence, it was the sum of “R1 head” and “R3 trochanter”). The ROIs are described in Table 2 and shown in Fig. 1.

The results from the simulation of X-rays were calculated for the three femoral bones. For each bone, the simulation was conducted in position of the bone (head right). Each bone was scanned by the DEXA and was imaged with the CT scanner.

Table 3
The settings of the CT scanner used during scanning the bone specimens

Setting name and unit	Value
Voltage (kVp)	120
Current (mA)	220
Scan time (s)	1
Slice thickness (mm)	3
Scan field of view (cm)	48
Table height (CT-table)	303 (=11.7 cm above isocentrum)
Reconstruction filter	Standard
Type of scan	Spiral Pitch = 1.5 Spacing = 3.0 mm Spiral interp.: standard
X-ray filter	Off

2.3. From QCT to virtual model of SDBD

The CT-data set was used to generate a voxel-model that had the same dimensions as the CT scan data set. In short, we used our own developed software which generated automatically a model of the SDBD based on the CT data set. The software provided automated detection of the calibration phantom in the CT images (Figs. 3 and 4) and extracted HU values and subsequently generated a calibration equation per CT-slice (Fig. 5). The software then virtually scanned in a straight line through the specimen which had a spatial distribution of density. Using a physics based attenuation algorithm (Section 2.4, formulas 1 and 2). More details about the calculation of the X-ray propagation is reported in our previous model published in 2006 [23]. Below, the steps to generate the virtual model with the spatial bony distribution are described in more detail.

2.3.1. Steps to generate the virtual model with the spatial bony distribution

The computer model of bone was constructed on the basis of the data from CT. In the scanning sessions, standard CT settings were applied, i.e. the settings which are commonly used in the examinations of human femora (Table 3). The bones were fixed in the water bath with a plastic holder in exactly the same horizontal position as during the previous DEXA tests (Fig. 2). The level of water in the bath was the same as well. A density phantom was placed under the water bath (Image Analysis Inc USA). Sixty-three to 113 (85 on average) transversal cross-sectional images were used to define one model of a femur. The resolution of all the data sets was constant; in all the models the voxel size was $0.97 \times 0.97 \times 3$ mm.

X-ray computed tomography delivers results as a collection of greyscale images. Usually, they are in the relative scale of Hounsfield Units, which represent the distribution of tissue densities in a cross-section. Fig. 3 shows a tomographic slice and its magnified region with a bone edge. Additionally, the density values in Hounsfield Units are included.

In this study the relative values were not sufficient to define bone density properly, as it should be defined in the mass per volume unit (g/cm^3). Since the quantitative information about bone density was required, the density phantom was used to

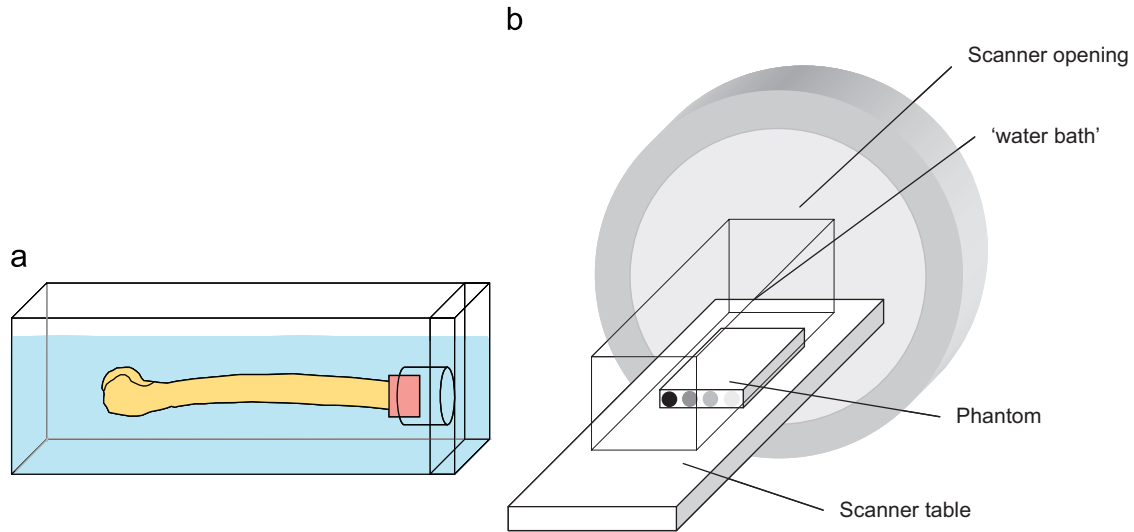


Fig. 2. A schematic drawing of the bone mounted in the water bath: (a) the water bath, (b) the water bath and the phantom on the CT scanner table.

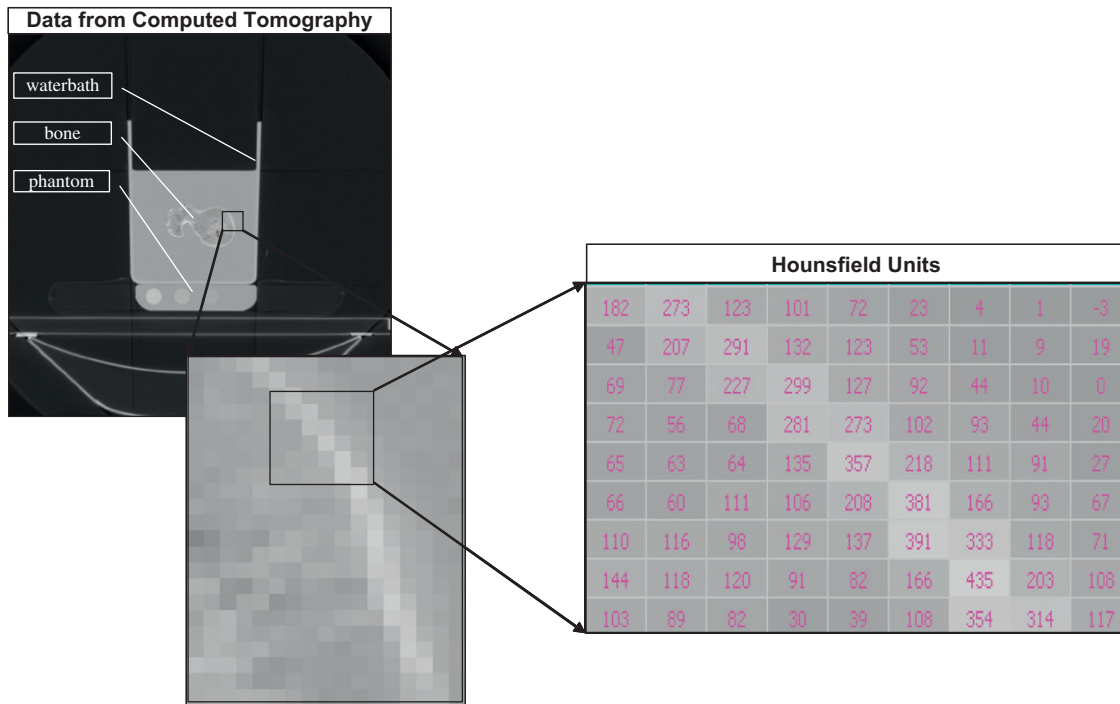


Fig. 3. A single cross-section of patient's bone or the data from scanning a bone in a water bath can be used for the assessment of the bone density. Hounsfield Units (HU) represent the density of the scanned object (within a relative scale). The units are commonly presented as grey levels in greyscale images, which is useful for diagnosis but can be used in a computer procedure of the bone density estimation as well.

convert the relative Hounsfield Units into real Ca–P equivalent density values.

The phantom contained four different materials, of which each represented a different value of Ca–P equivalent density: 200, 100, 50, and 0 mg/cm³. The phantom was placed under the water bath; it was visible on each reconstructed CT slice (Figs. 3–5). Hence, a calibration curve could be constructed linking the HU units to actual Ca–P equivalent density values (in (g/cm³)). Such an operation was performed for every

cross-section image of the bone, which permitted avoiding errors caused by different representations of real density with grey values on the individual images.

Next, for a selected cross-section, the values of real bone density were calculated according to the calibration curve for this cross-section. In this way, the spatial distribution of the Ca–P equivalent density of the tested bones was determined. This enabled reconstruction of the three-dimensional bone model in the simulation space.

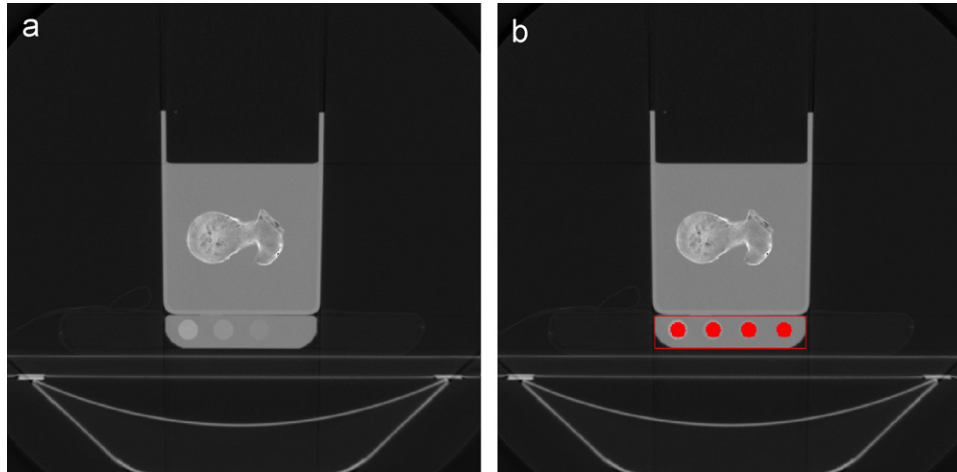


Fig. 4. Tomographic images of a bone specimen: (a) a transversal cross-sectional image of a bone scanned in a water bath, under the bath there is a density phantom; and (b) 4 points of the phantom selected using an automatic procedure.

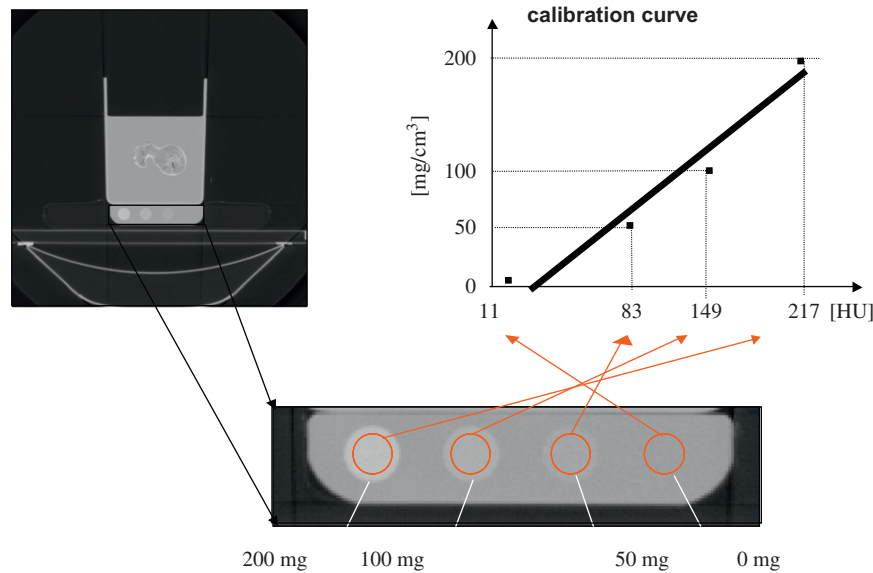


Fig. 5. An example of the calibration curve. It was created using the HU values from four circular regions (each of different density). Linear regression was used to find a linear function best fitted to the four points. We call this function the calibration curve.

2.4. Calculation of the X-ray radiation propagation through the bone model in the simulation

In this study we employed an improved method relative to our earlier work [23] by adding a calibration curve to achieve more accurate calculations of the physical bone density, which resulted in a better estimation of the X-ray attenuation coefficient. The precise estimation of this parameter was crucial for improving the quality of the results from the entire simulation; a small error in the attenuation coefficient value would significantly influence the accuracy of the results.

The model of the X-ray propagation in densitometry equipment was based on the Lambert Beer law [8,12,14,33]. This law defines an exponential formula describing the X-ray radiation intensity after transition through a layer of matter as a function of the layer thickness and its X-ray attenuation coefficient.

The propagation of X-rays was modelled in a virtual discrete simulation space. The space is defined in a rectangular three-dimensional coordinate system (x, y, z). The system has a cubic shape and the dimensions of [0..X, 0..Y, 0..Z]. For each axis a minimal unit (dx, dy, dz) is defined. It determines the size of the basic computational unit—a voxel—and, consequently, the resolution of the computations.

The top and bottom layers of the simulation space function as the source and the detector of X rays. Each voxel that belongs to the source layer is an elementary X-ray source. Similarly, voxels in the detector layer are elementary X-ray detectors. The parallel geometry of X-ray propagation is assumed—a voxel of the detector receives only the radiation emitted by the respective voxel of the source.

The SDBD model is located in the simulation space between the source and detector layer. The model defines the physical

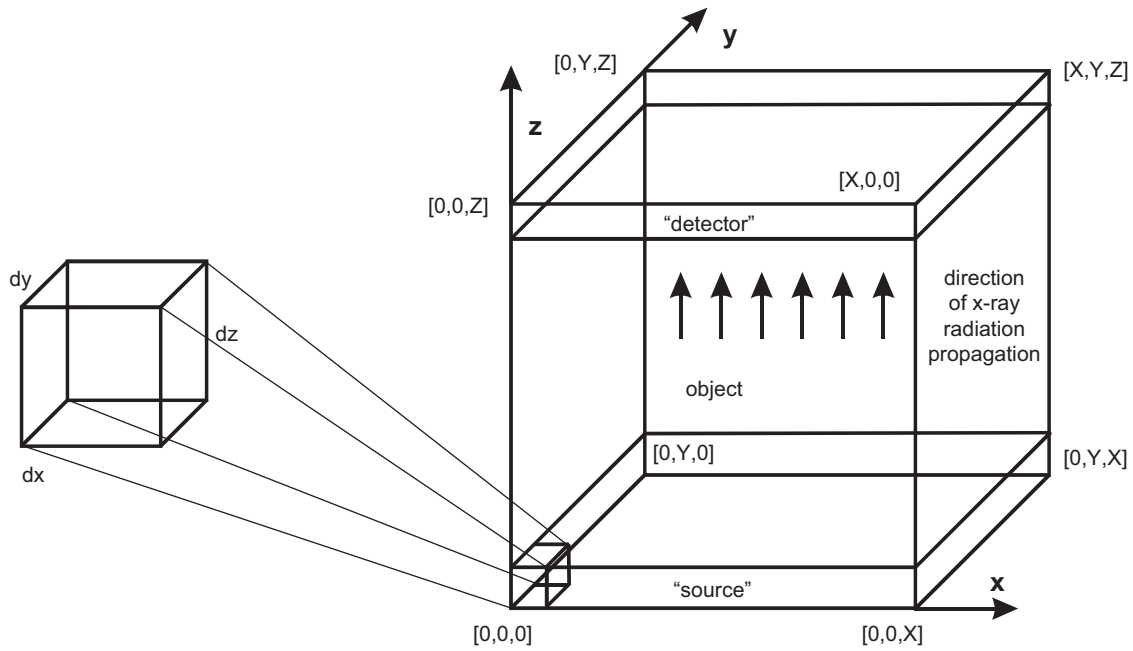


Fig. 6. The schematic diagram of the simulation space and a single voxel of this space.

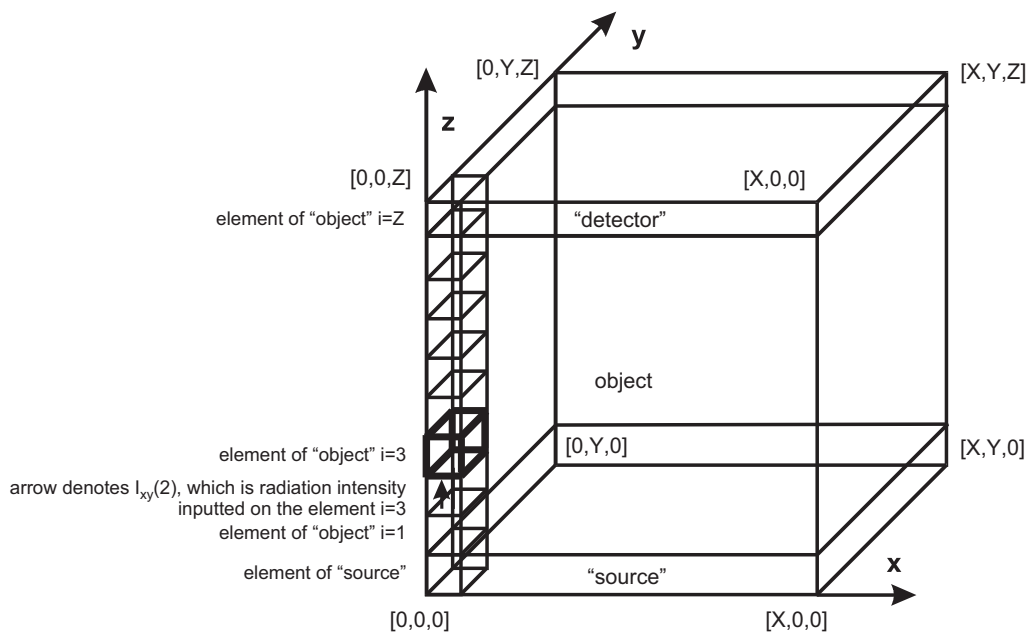


Fig. 7. The schematic diagram of the simulation space and a single column of the voxels for which iterative calculation of the X-ray intensity is performed.

bone density for its voxels. Based on this data the X-ray attenuation coefficient is computed for the voxels of simulation space.

The radiation intensity in the detector elements is calculated in an iterative way. For each voxel on a X-ray path between the source and detector the radiation intensity in a voxel (i) is calculated on the basis of the intensity from the previous voxel ($i - 1$).

The schematic diagram of the simulation space and a voxel of this space is shown on Fig. 6, Formula (1) presents the

iterative formula used to calculate the radiation intensity for a single voxel (Fig. 7).

$$I_{xy}(i) = I_{xy}(i - 1) \exp(-\mu(i)l) \tag{1}$$

where $I_{xy}(i)$ is the radiation intensity after transition through the current voxel (i) of SDBD model, $I_{xy}(i - 1)$ the radiation intensity for the voxel ($i - 1$), which was computed in the previous iteration, $\mu(i)$ the linear factor of absorption for the current voxel of the SDBD model, and l the thickness of the voxel

Table 4

The comparison of the results from the X-ray simulation with the results from the real densitometry tests for bone no. 1, acquired for four different ROIs

Bone 1														
Region of Interest			DEXA			Simulation			Differences					
Name	Width (mm)	Height (mm)	Area (cm ²)	BMC (g)	BMD (g/cm ²)	Area (cm ²)	BMC (g)	BMD (g/cm ²)	Area		BMC		BMD	
									(cm ²)	(%)	(g)	(%)	(g/cm ²)	(%)
R1 head	125	49	35.75	27.84	0.779	38.00	27.63	0.727	-2.25	-6.3	0.21	0.8	0.05	6.7
R2 neck	125	25	23.86	17.97	0.753	24.08	17.26	0.717	-0.22	-0.9	0.71	4.0	0.04	4.8
R3 Trochanter	125	60	28.15	27.7	0.984	31.93	29.99	0.939	-3.78	-13.4	-2.29	-8.3	0.05	4.6
R4 all	125	108	63.14	54.97	0.871	67.00	55.67	0.831	-3.86	-6.1	-0.70	-1.3	0.04	4.6

in the direction of the radiation propagation. The thickness was the same in the entire model.

The X-ray attenuation coefficient μ_i is the sum of the absorption and attenuation that occur during the interaction of the radiation with matter.

$$\mu_i = \sigma_i + \tau_i + \sigma_{ri} + \pi_i + \gamma_i \quad (2)$$

where σ_i is the Compton attenuation coefficient, τ_i the attenuation coefficient for photoelectric effect, σ_{ri} the Rayleigh scatter attenuation coefficient, π_i the pair production attenuation coefficient, and γ_i the triplet attenuation coefficient.

Taking into consideration the fact that in medical diagnosis techniques, such as computed tomography or micro computed tomography, the applied X-ray energy lies between 20 and 150 keV, three most important interactions which have influence on the attenuation of X rays can be distinguished: the photoelectric effect, Compton scattering and coherent scattering. In our area of interest the Compton scattering effect is the most important one. The influence of other interactions in biological materials constitutes less than 3% of the whole attenuation [14].

The final attenuation for a voxel depends on the density measured for this voxel and an attenuation coefficient defined on the basis of the data available in the literature, i.e. the table containing the value of coefficients depending on the energy of photons, obtained from empirical research [11].

2.5. Calculation of the densitometry parameters in the simulation

On the basis of the model of X-ray propagation the results for the detector were calculated as a distribution of the X-ray intensity—a two-dimensional matrix of radiation intensities lighting the detector. For a certain region of interest, a densitometry parameter called Area (cm²) was estimated. It was obtained by measuring the radiation intensity in the parts of the detector where the radiation was not attenuated by the bone. In the detected area of the bone, for every point of the detector the value of intensity was used to calculate the attenuation effect. A logarithmic function of the detector was used to obtain components to calculate (for a certain bone area) the densitometry parameter called the BMD (g/cm²). Based on two previously

calculated parameters (area and BMD) the BMC (g) was calculated.

3. Results

Bones were modelled using CT data. The ROI's are defined on the basis of the same anatomical features (see Table 2), the areas of the ROI's for the individual bones depend on the bone size and so does the area parameter. Moreover, it is also the bone shape that influences the area parameter, independently of the ROI area. Since area varies, the comparison of the results for bones must be performed for all three densitometry parameters.

In Tables 4–6 the obtained results for bones (for the position with the head turned right) are compared with the DEXA results. Percentage differences between the results from DEXA and the simulation were calculated as well.

We can see that the area parameter exhibits the highest percentage differences for each bone. Predominantly, the calculated Area is bigger than one obtained from DEXA. For the maximal negative percentage differences it led to the underestimation of the BMC parameter. The causes of the inaccuracies in the Area calculation are discussed in the next section.

When the results of R1, R2, and R3 of the simulation were correlated with those of the DEXA experiments, very high correlations were found (Figs. 8 and 9). The R-square values for the AREA and BMC were 0.98 and 0.99, respectively. In addition, the equations showed that the offsets of the lines were almost zero and the slopes almost 1.0 (Figs. 8 and 9).

4. Discussions

The proposed method has some intrinsic limitations, which can impair the correspondence between the modelled and real DEXA results. First of all, we simulate 'ideal' DEXA equipment according to its physical model. In the real equipment used to verify the obtained simulation results several parameters remain unknown. In particular, there was no information available about the amplifier or physical properties of the source and detector of the DEXA equipment. Moreover, the behaviour of the DEXA equipment was sometimes rather unpredictable, as we recorded in the case of one bone where automatic ROI selection failed.

Table 5
The comparison of the results from the X-ray simulation with the results from the real densitometry tests for bone no. 2, acquired for four different ROIs

Region of Interest		DEXA				Simulation			Differences					
Name	Width (mm)	Height (mm)	Area (cm ²)	BMC (g)	BMD (g/cm ²)	Area (cm ²)	BMC (g)	BMD (g/cm ²)	Area		BMC		BMD	
									(cm ²)	(%)	(g)	(%)	(g/cm ²)	(%)
R1 head	125	36	17.52	8.21	0.469	18.4	8.12	0.441	-0.88	-5.0	0.09	1.1	0.03	6.0
R2 neck	125	13	8.75	3.57	0.408	9.2	3.69	0.401	-0.45	-5.1	-0.12	-3.4	0.01	1.7
R3 Trochanter	125	47	20.52	11.11	0.542	21.39	11.79	0.551	-0.87	-4.2	-0.68	-6.1	-0.01	-1.7
R4 all	125	82	37.44	19.08	0.51	41.6	20.65	0.496	-4.16	-11.1	-1.57	-8.2	0.01	2.7

Table 6
The comparison of the results from the X-ray simulation with the results from the real densitometry tests for bone no. 3, acquired for four different ROIs

Region of Interest		DEXA				Simulation			Differences					
Name	Width (mm)	Height (mm)	Area (cm ²)	BMC (g)	BMD (g/cm ²)	Area (cm ²)	BMC (g)	BMD (g/cm ²)	Area		BMC		BMD	
									(cm ²)	(%)	(g)	(%)	(g/cm ²)	(%)
R1 head	125	55	38.42	13.18	0.343	38.35	12.91	0.337	0.07	0.2	0.27	0.2	0.01	1.7
R2 neck	125	35	30.55	9.1	0.298	29.68	8.79	0.296	0.87	2.8	0.31	3.4	0.00	0.7
R3 Trochanter	125	43	21	6.62	0.315	21.5	8.46	0.393	-0.50	-2.4	-1.84	-27.8	-0.08	-24.8
R4 all	125	97	58.7	19.61	0.334	59.85	21.36	0.357	-1.15	-2.0	-1.75	-8.9	-0.02	-6.9

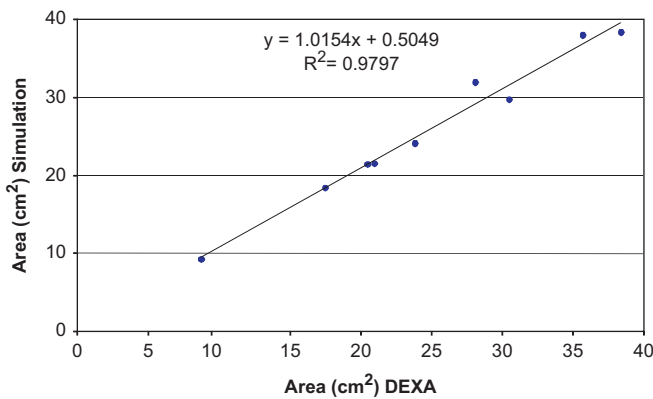


Fig. 8. Correlation of the area between the simulated and DEXA measurement. Note that the correlation is high, the offset is almost zero, and the slope is almost 1.0.

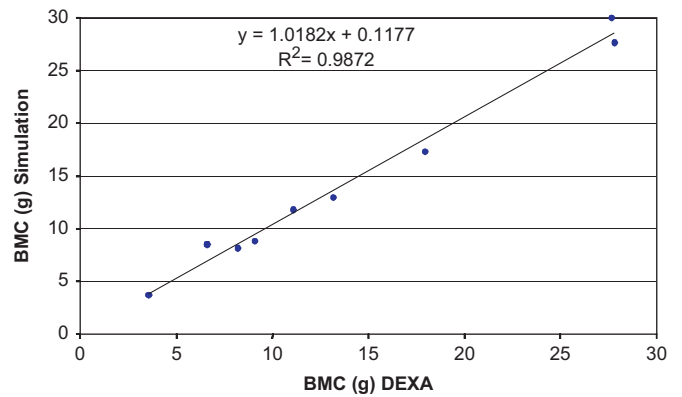


Fig. 9. Correlation of the BMC between the simulated and DEXA measurement. Note that the correlation is high, the offset is almost zero, and the slope is almost 1.0.

During the tests, there were problems with the detection of the bone area in the case of bone no. 3. This bone had very low parameters of density and the DEXA software was not able to determine the bone area automatically. Therefore, we performed the bone image extraction manually. Obviously, the manual procedure depended on the operator and his arbitrary decision where the edge of a bone was. This led to a significantly larger difference between the results from DEXA and the simulation. In the remaining cases, i.e. for bone no. 1 and 2, the results of automatic bone image extraction were

satisfactory. The problems encountered with bone no. 3 show that the DEXA method may have limitation in ROI's that are truly of very low density. For these regions the DEXA software cannot determine the borders of the region and therefore creates errors in the actual area of the region (and its BMD).

Another source of discrepancies between the real and modelled results is the resolution of the data used to create the SDBD model (i.e. the bone model). In this study we used a relatively coarse 3 mm slice-to-slice resolution in the CT scans, whereas the DEXA resolution was 1 mm line spacing. Although

these resolution differences do not influence density calculations on a global level, they do cause problems with determining the exact position of a bone and hence makes it difficult to calculate the Area and (consequently) BMD densitometry parameters precisely.

Finally, the proposed model of X-ray propagation does not cover all the physical phenomena, such as the full spectrum of the X-ray source, a real detector instead of the ideal one, the fan or cone X-ray beam geometry and the stochastic calculation of X-ray interactions with bone tissue.

In the presented comparison, the largest difference was observed for the Area parameter. Unfortunately, it was not possible to set the size of the voxel reconstructed from the tomographic data equal to the densitometer resolution. The method of bone area determination, which is connected with the voxel area size in both methods, was an important limitation of our approach. In the tomographic data the distance between slices of 3mm was rather large, which led to errors in the estimation of the total bone area, whereas in DEXA the line spacing of 1 mm caused a series of problems with bone position determining.

Although the sample size is three, it covers a range of bone densities that are typically assessed when one wants to acquire information about the bone quality. In addition, we analysed different regions per bone which came down to a total of nine regions of which we could compare the simulation results with the experimental (true DEXA) findings. Therefore, including another bone (or more) would most likely not change any outcome of this study.

This study showed that the simulation of X-rays and the following calculation of densitometry parameters were in accordance with the results from the real diagnostic technique. Consequently, it shows that the simulation of densitometry techniques is possible and could be applied in the computer analysis of densitometry tests of bone tissue.

5. Conclusions

Generally speaking, the results from the simulation of X-rays adequately match the results from the DEXA tests. The simulation produced results that highly correlated with the DEXA experiments; *R*-square values for the AREA and BMC were 0.98 and 0.99, respectively. There were several reasons why the simulation is not perfect but, on the other hand, some features of DEXA techniques are difficult to repeat in a physical model of X-ray propagation as well as in the calculation of densitometry parameters.

Nonetheless, considering the simplicity of the models, the results are satisfactory. If all the parameters of the components used in the densitometer were known, it would be reasonable to consider several improvements to the model, for instance implementing a detector of a real absorbing capability. In addition, a full implementation of the physics in the densitometry model could also include: the pencil beam or cone beam propagation geometry, the computation model of X-ray radiation that takes into account all the interactions of X rays with matter and the X-ray source model featuring the X-ray spectrum.

Furthermore, the models should be defined taking into account stochastic phenomena.

Another issue is introducing improvements to the SDBD model. It should be noted that when a computer simulation is based on tomographic data, it is possible to calculate physical density very accurately, although errors will also be generated in the CT quantification as a result of beam hardening, positioning effects, effects of energy levels, etc. The details of this issue, however, remain beyond the scope of this paper.

Finally, we can conclude that the main goal of our research was achieved. During the validation process we proved that the simulation of X-rays and the following calculation of densitometry parameters are in accordance with the results from the real diagnostic technique. Consequently, it proves that the simulation of densitometry techniques is possible and could be applied in the computer analysis of densitometry tests of bone tissue.

Conflict of interest statement

None declared.

Acknowledgments

M. Binkowski is the holder of the Young Scientists Scholarship (2006) from the Foundation for Polish Science which allowed him to do this research. This study was partly sponsored by a grant from the Dutch Science Foundation (STW). Project number: NPG.6778.

References

- [1] WHO, Assessment of Fracture Risk and its Applications to Screening for Postmenopausal Osteoporosis, World Health Organization, Geneva, Switzerland, 1994.
- [2] J.A. Kanis, O. Johnell, A. Oden, H. Johansson, J.A. Eisman, S. Fujiwara, H. Kroger, R. Honkanen, L.J. Melton III, T. O'Neill, J. Reeve, A. Silman, A. Tenenhouse, The use of multiple sites for the diagnosis of osteoporosis, *Osteoporos. Int.* 17 (2006) 527–534.
- [3] O. Johnell, J.A. Kanis, A. Oden, H. Johansson, C. De Laet, P. Delmas, J.A. Eisman, S. Fujiwara, H. Kroger, D. Mellstrom, P.J. Meunier, L.J. Melton III, T. O'Neill, H. Pols, J. Reeve, S. Silman, A. Tenenhouse, Predictive value of BMD for hip and other fractures, *J. Bone Miner. Res.* 20 (2005) 1185–1194.
- [4] J.A. Kanis, F. Borgstrom, N. Zethraeus, O. Johnell, A. Oden, B. Jonsson, Intervention thresholds for osteoporosis in the UK, *Bone* 36 (2005) 22–32.
- [5] O. Johnell, J.A. Kanis, A. Oden, I. Sernbo, I. Redlund-Johnell, C. Pettersson, C. De Laet, B. Jonsson, Fracture risk following an osteoporotic fracture, *Osteoporos. Int.* 15 (2004) 175–179.
- [6] J.A. Kanis, O. Johnell, A. Oden, B. Jonsson, C. De Laet, A. Dawson, Risk of hip fracture according to the World Health Organization criteria for osteopenia and osteoporosis, *Bone* 27 (2000) 585–590.
- [7] J. Badurski, A. Sawicki, S. Boczoń, *Osteoporosis, Osteoprint*, Białystok, Poland, 2006.
- [8] V.C. Mow, R. Huiskes, *Basic Orthopaedic Biomechanics and Mechano-Biology*, Lippincott Williams & Wilkins, Philadelphia, Baltimore, New York, London, Buenos Aires, Hong Kong, Sydney, Tokyo, 2005.
- [9] E. Czerwiński, P. Działak, Diagnostyka osteoporozy i ocean ryzyka złamania, *Ortoped. Traumatol. Rehabil.* 4 (2002) 127–134.

- [10] H. Burger, C.E. de Laet, P.L. van Daele, A.E. Weel, J.C. Witteman, A. Hofman, H.A. Pols, Risk factors for increased bone loss in an elderly population: the Rotterdam Study, *Am. J. Epidemiol.* 147 (1998) 871–879.
- [11] A. Nowak, J. Badurski, Białystok Osteoporosis Study (BOS): epidemiology of low trauma fractures in the female population, *Osteoporos. Int.* 12 (2001) (Suppl. 1) L03.
- [12] J. Beutel, H.L. Kundel, R.L. Van Metter, *Handbook of Medical Imaging, Physics and Psychophysics*. SPIE Press, 2000.
- [13] S.C. Cowin, *Bone Mechanics Handbook*, CRC Press, London, New York, Washington, DC, 2001.
- [14] W.R. Hendee, E.R. Ritenour, *Medical Image Physics*, Wiley-Liss, New York, 2002.
- [15] M. Pawlikowski, T. Niedźwiecki, *Mineralogia Kości*, PAN Oddział w Krakowie, Poland, 2002.
- [16] Z. Bliznakov, G. Pappous, K. Bliznakova, N. Pallikarakis, Integrated software system for improving medical equipment management, *Biomed. Instrum. Technol.* 37 (2003) 25–33.
- [17] D. Lazos, K. Bliznakova, Z. Kolitsi, N. Pallikarakis, An integrated research tool for X-ray imaging simulation, *Comput. Methods Programs Biomed.* 70 (2003) 241–251.
- [18] D. Lazos, Z. Kolitsi, N. Pallikarakis, A software data generator for radiographic imaging investigations, *IEEE Trans. Inf. Technol. Biomed.* 4 (2000) 76–79.
- [19] K. Bliznakova, Z. Bliznakov, V. Bravou, Z. Kolitsi, N. Pallikarakis, A three-dimensional breast software phantom for mammography simulation, *Phys. Med. Biol.* 48 (2003) 3699–3719.
- [20] K. Bliznakova, Z. Kolitsi, N. Pallikarakis, Dual-energy mammography: simulation studies, *Phys. Med. Biol.* 51 (2006) 4497–4515.
- [21] G.J. Michael, C.J. Henderson, Simulation studies of optimum energies for DXA: dependence on tissue type, patient size and dose model, *Australas. Phys. Eng. Sci. Med.* 22 (1999) 126–135.
- [22] G.J. Michael, C.J. Henderson, Monte Carlo modelling of an extended DXA technique, *Phys. Med. Biol.* 43 (1998) 2583–2596.
- [23] M. Binkowski, A. Dyszkiewicz, Z. Wrobel, The analysis of densitometry image of bone tissue based on computer simulation of X-ray radiation propagation through plate model, *Comput. Biol. Med.* 37 (2006) 245–250.
- [24] D. Lazos, Z. Kolitsi, N. Pallikarakis, Monte Carlo simulation of the radiographic imaging procedure for electronically designed phantoms, *Stud. Health Technol. Inform.* 68 (1999) 391–394.
- [25] D. Lazos, Z. Kolitsi, N. Pallikarakis, A software data generator for radiographic imaging investigations, *IEEE Trans. Inf. Technol. Biomed.* 4 (2000) 76–79.
- [26] M. Meta, Y. Lu, J.H. Keyak, T. Lang, Young-elderly differences in bone density, geometry and strength indices depend on proximal femur sub-region: a cross sectional study in Caucasian–American women, *Bone* 39 (2006) 152–158.
- [27] J.H. Keyak, T.S. Kaneko, J. Tehranzadeh, H.B. Skinner, Predicting proximal femoral strength using structural engineering models, *Clin. Orthop. Relat Res.* (2005) 219–228.
- [28] J.H. Keyak, T.S. Kaneko, S.A. Rossi, M.R. Pejicic, J. Tehranzadeh, H.B. Skinner, Predicting the strength of femoral shafts with and without metastatic lesions, *Clin. Orthop. Relat Res.* 439 (2005) 161–170.
- [29] T.S. Kaneko, J.S. Bell, M.R. Pejicic, J. Tehranzadeh, J.H. Keyak, Mechanical properties density and quantitative CT scan data of trabecular bone with and without metastases, *J. Biomech.* 37 (2004) 523–530.
- [30] T.S. Kaneko, M.R. Pejicic, J. Tehranzadeh, J.H. Keyak, Relationships between material properties and CT scan data of cortical bone with and without metastatic lesions, *Med. Eng. Phys.* 25 (2003) 445–454.
- [31] C.M. Les, S.M. Stover, J.H. Keyak, K.T. Taylor, A.J. Kaneps, Stiff and strong compressive properties are associated with brittle post-yield behavior in equine compact bone material, *J. Orthop. Res.* 20 (2002) 607–614.
- [32] J.H. Keyak, S.A. Rossi, K.A. Jones, C.M. Les, H.B. Skinner, Prediction of fracture location in the proximal femur using finite element models, *Med. Eng. Phys.* 23 (2001) 657–664.
- [33] C.M. Langton, C.F. Njeh, *The Physical Measurement of Bone*, Institute of Physics, Bristol and Philadelphia, 2004.
- [34] J.H. Hubbell, S.M. Seltz, *Tables of X-Ray Mass Attenuation Coefficients and Mass Energy-Absorption Coefficients from 1 KeV to 20 MeV for Elements Z=1 to 92 and 48 Additional Substances of dosimetric Interest*, National Institute of Standards and Technology, 1996.

Marcin Binkowski is a lecturer at the Department of Biomedical Computer Systems at the Institute of Computer Sciences, University of Silesia, Poland. He received his Ph.D. degree in Biomedical Engineering from the Institute of Biocybernetics and Biomedical Engineering, Polish Academy of Sciences, Poland (2007). He was awarded a Scholarship for Young Scientists (2006) and Columb Programme to support a Postdoctoral Out-Going Fellowships (2007–08) from the Foundation for Polish Science. He is currently working as a Honorary Senior Research Fellow in the Institute of Orthopaedics and Musculoskeletal Science in University College London, United Kingdom. His research interests include: modelling of bone tissue, computer simulations, medical imaging and software development.

Esther Tanck is a lecturer at the Orthopaedic Research Laboratory at the Radboud University Nijmegen Medical Center, The Netherlands. She received her Ph.D. degree in Medical Sciences on the subject ‘Mechanical regulation of bone development’ at the Radboud University Nijmegen Medical Center, The Netherlands. Her research interests include: bone metastases, osteoporosis, imaging, fracture prediction using Finite Element models.

Marco Barink is project lead numerical simulations at the department of Materials Performance of TNO Science and Industry (Dutch Organization for Applied Scientific Research), Eindhoven, The Netherlands. He received his Ph.D. degree in 2007 at the Radboud University Nijmegen, The Netherlands. His Ph.D. Thesis was entitled ‘Design improvements in Total Knee Arthroplasty’. His research interests include: experimental and numerical material behaviour and biomedical research.

Wim Oyen is professor of Nuclear Medicine and head of the Department of Nuclear Medicine at Radboud University Nijmegen Medical Centre, Nijmegen, The Netherlands. His research interests include multimodality molecular imaging, image analysis and targeted therapies.

Zygmunt Wróbel is the Head of the Department of Biomedical Computer Systems at the Institute of Computer Sciences, Silesian University, Poland. He received his Ph.D. in Physics from Silesian University (1976) and attained Habilitation in Electronic Sciences at Silesian University of Technology, Poland (1996). His research interests include: the computer analysis and processing of biomedical images and signals, the application of information technology in medicine and biotechnology.

Nico Verdonchot is professor of Implant Biomechanics at the Orthopaedic Research Laboratory, Radboud University Nijmegen Medical Centre, Nijmegen, The Netherlands and has also a position at the Department of Bioengineering, University of Twente, The Netherlands. His research interests focus on testing and computer simulations of orthopaedic implants and bone fractures.